American Mineralogist, Volume 75, pages 1120–1139, 1990

Mechanisms and kinetics of apatite fission-track annealing

William D. Carlson
Department of Geological Sciences, University of Texas at Austin, Austin, Texas 78713, U.S.A.

Abstract

Kinetic equations derived from a physical model of the atomic-scale processes involved in apatite fission-track annealing account for the dependence of annealing rates on temperature and time over the full range of these variables investigated experimentally to date. The physical model postulates radial shrinkage of the disrupted zone surrounding the path of the fission fragments, in response to the elimination of crystalline defects by short-range atomic repositioning during thermal annealing. For the case of a disrupted zone that is cylindrical near its axial center with regions of conical taper at each end, the model predicts a two-stage annealing process in which track-length reduction is dominated initially by axial shortening, and subsequently by segmentation of tracks. The kinetics of the axial-shortening mechanism are determined by three parameters that quantify the spatial distribution of defects, the activation energy for the atomic motions required to eliminate defects, and a rate constant that incorporates factors for the geometry of the track tip. The kinetics of the segmentation mechanism are determined by a single additional parameter that quantifies, as a function of the mean track length, the fraction of the total number of tracks that have been segmented. The model reproduces laboratory annealing data with an accuracy nearly equal to the uncertainty of the experimental measurements.

Although the dependence of annealing rates on apatite composition cannot be accurately deduced from the experimental data presently available, an analogy to rates of O diffusion in silicates suggests that the kinetic parameters of the model may vary with composition as linear functions of the total ionic porosity. This prediction is in qualitative agreement with limited experimental data and with the relative rates of annealing observed for apatite of different composition in natural occurrences. Experimental indications of annealing anisotropy can be explained under this model by invoking small differences in the geometry of the disrupted zone for different crystallographic orientations.

Because this kinetic model is based on explicit physical mechanisms, extrapolations of annealing rates to the lower temperatures and longer time scales required for the interpretation of natural fission-track length distributions can be made with greater confidence than is the case for purely empirical relationships fitted to the experimental annealing data.

Introduction

Fission tracks form continuously in uraniferous apatite but shorten and eventually disappear in response to heating in the temperature range of approximately 25–150 °C. As a result, the frequency distribution of track lengths in apatite is potentially a sensitive monitor of a crystal's thermal history throughout a range of temperatures that is critical to numerous processes in the upper crust, including basin subsidence and uplift, erosional unroofing and shallow tectonism during orogeny, hydrothermal alteration, and the maturation of hydrocarbons in sedimentary basins. In addition, the track-length distribution and its response to thermal episodes directly influence the revelation and persistence of tracks from which fission-track ages are determined, so a quantitative understanding of the annealing process is essential to the interpretation of apatite fission-track ages. These considerations have recently led to a burgeoning effort to quantify the kinetics of apatite fission-track (AFT) annealing on the basis of laboratory experiments in which track-length distributions are measured in crystals subjected to controlled thermal histories (e.g., Green et al., 1986, 1989; Laslett et al., 1987; Duddy et al., 1988; Donelick, 1988).

The application of experimental studies to natural occurrences, however, depends critically upon the extrapolations required: temperatures of laboratory experiments are 100–200 °C higher than those of interest in nature, and even more perniciously, laboratory data measured over roughly four orders of magnitude in time must be extrapolated over as much as ten or more additional orders of magnitude to reach geological time scales. Quantitative interpretations based on such extrapolations are perilous in any case, but they are made all the more

0003–004X/90/0910–1120$02.00

so in the instance of AFT annealing by the fact that no physical mechanism for the annealing process has been identified that yields quantitative predictions of annealing rates. As a result, all treatments to date have been purely empirical, based upon mathematical features of laboratory results without clear physical significance. This article attempts to provide a more reliable basis for the application of laboratory annealing data to natural occurrences by examining, from a mineralogical standpoint, the physical mechanisms operating at the atomic scale during the thermal annealing of fission tracks in apatite.

Annealing produces reductions in etchable track lengths at rates that have been shown experimentally to be complex functions of temperature, time, the anionic composition of the apatite, and the crystallographic orientation of the track. Qualitatively, the dependence of AFT annealing rates on these factors is well characterized, as follows. (1) In experimental studies, rates of track shortening have been shown to increase exponentially with rising temperature: for example, the data of Green et al. (1986) show that the time required to reduce the mean track length by 1 μm at 258 °C is 36000 times shorter than the time required for the same reduction in track length at 123 °C. (2) Annealing rates in isothermal experiments decline abruptly over time: for example, the data of Green et al. (1986) show that at 210 °C, an initial 1-μm reduction in track length occurs in the first hour, whereas a further 1-μm reduction requires about 100 h at this temperature. (3) Annealing rates have also been shown experimentally to depend appreciably upon apatite composition: for example, Green et al. (1985) and Crowley and Cameron (1987) document that tracks in Cl-rich apatites anneal more slowly than do those in OH- and F-rich apatites. (4) Finally, annealing rates as revealed by etched track lengths depend upon the crystallographic orientation of the tracks: for example, Donelick (1988), among many others, has demonstrated that fission tracks parallel to the c axis in apatite shorten more slowly than do tracks perpendicular to it.

The intent of this article is to provide a physical explanation for these observations using a kinetic model based upon an atomic-scale description of the process of fission-track annealing. The premise underlying the model presented here is that the mechanisms involved in fission-track annealing bear strong resemblances to the better-understood mechanisms involved in topotactic mineral transformations and in O diffusion in silicates. These processes share with AFT annealing an exponential temperature dependence of rate; the former has an orientation dependence of rate analogous to that seen in AFT annealing, whereas the latter has a dependence of rate upon composition and structure analogous to that seen in AFT annealing.

To exploit these similarities, the next section of this article briefly reviews pertinent observations and deductions concerning the nature of fission-track damage. The subsequent section presents an idealized atomic description of apatite fission-track annealing and derives from it equations for the rate of shortening of fission tracks in apatite as a function of time and temperature. These equations are verified against the experimental data base presently available. The next two sections propose means of generalizing the kinetic equations to account for variations in apatite composition and for variations in crystallographic orientation, and in the final section of the paper this kinetic model is compared to previously published models.

Background

A latent (unetched) fission track in apatite is envisioned as a zone of disrupted crystal structure surrounding the linear path of the fission fragments. The atomic interactions that generate the disrupted zone are complex and incompletely understood; for reviews, consult Fleischer et al. (1975, p. 3–49) and Chadderton (1988). Disrupted regions in the apatite contain, by comparison to the original structure, a markedly increased density of defects, predominantly vacancies and interstitial atoms. Small-angle X-ray and neutron scattering studies of tracks in experimentally irradiated minerals (e.g., Dartyge et al., 1981; Albrecht et al., 1984, 1985) lead to the inferences that disrupted zones are approximately cylindrical, that the variation in defect density radially across them is approximately Gaussian, and that their diameters are on the order of several tens of ångströms. Diameters of this magnitude are consistent with high-resolution transmission electron microscopic (HRTEM) observations of charged-particle tracks in several minerals and synthetic materials (e.g., Yada et al., 1987; Chadderton, 1988; Chadderton et al., 1988; Thiel et al., 1988; Houpert et al., 1988). These dimensions for the disrupted zones that make up latent tracks should not be confused with the dimensions of tracks made optically visible by chemical etching, in which dissolution extending beyond the disrupted zone has opened cylinders or cones with diameters of fractions of a micrometer to several micrometers.

All further deductions concerning the nature of fission-track damage are, to varying degrees, conjectural because only a modicum of agreement exists among attempts to characterize the disrupted zone of a nuclear track in greater detail. Dartyge et al. (1981) concluded from small-angle X-ray scattering studies and etching-rate measurements that tracks in experimentally irradiated silicates can be either intermittent or continuous along their length, traits exemplified respectively by tracks in muscovite and in feldspar. Toulemonde et al. (1989) interpreted HRTEM images of latent tracks in insulating magnetic oxides as evidence that the degree of continuity of tracks in a given material is a direct function of the material's electronic stopping power for a particular ion. However, the model for intermittency of Dartyge et al., which invokes large clusters of defects (extended defects) alternating along the tracks' length with individual point defects, has been called into question: Albrecht et al. (1985) were unable to observe any clusters of defects in muscovite, and the analysis of Chadderton et al. (1988) attributes the intermit-

tent nature of tracks in muscovite simply to the strong anisotropy of the layered crystalline structure of mica. Correspondingly, the study of feldspar by Dartyge et al. and most published work on tracks in substances of less extreme anisotropy than mica (e.g., Albrecht et al., 1984, 1985; Fuchs et al., 1987; Thiel et al., 1988; Houpert et al., 1988) take the view that nuclear tracks in more nearly isotropic substances are closely approximated by continuous regions of disruption.

Although observations bearing on the degree of continuity of unannealed fission tracks in apatite are less numerous, it is probable that the moderate anisotropy of the apatite crystal structure is insufficient to produce distinctly intermittent disrupted zones. Green et al. (1986) sought direct evidence for the presence of discontinuities or gaps in both unannealed and annealed tracks in apatite. They indicate that there is no evidence for unetchable gaps in unannealed samples (their Fig. 9), although such gaps may develop in heavily annealed samples (their Fig. 10). The meager data now available are therefore interpreted here as evidence that the distribution of fission-track damage in apatite is closely approximated by a continuous, approximately cylindrical zone of disruption.

Two kinetically distinct stages of AFT annealing were first identified in the experimental study of Green et al. (1985). The first stage is characterized by a systematic reduction in mean etchable track length after controlled periods of annealing at fixed temperatures, which continues until the mean track length has been reduced to approximately 11 μm, that is, to about two-thirds of its original value. Further annealing produces greatly accelerated reductions in mean etchable track lengths, accompanied by a markedly increased dispersion of track lengths about their mean (Green et al., 1985, p. 326 and their Fig. 3). The experimental annealing data of Green et al. (1986) and Donelick (1988) also show a marked acceleration of annealing rates and an increased dispersion of track lengths at advanced stages of annealing; in the latter study, this change is coupled with an abrupt change in the systematics of the orientational dependence of annealing rate.

Green et al. (1986, p. 249) interpreted the first stage of annealing as the result of healing of tracks from their ends inward toward their centers, and they interpreted the second stage as the result of both anisotropy of annealing of tracks in different orientations and the development during annealing of unetchable gaps in the tracks. Because fission tracks pass quickly through the relatively brief second stage shortly before fading completely, tracks in this stage of annealing will be preserved only rarely in natural occurrences.

It should be recognized that all of the observations recounted above are subject to diverse interpretations, and in some cases, conflicting conclusions have been reached from them in the literature. In many instances, this is the result of the unavoidable necessity of using measurements on etched tracks to deduce characteristics of latent tracks. The convolution of the kinetics of chemical etching with the kinetics of track annealing may introduce a host of additional complications, few of which have been thoroughly explored (cf. Dartyge et al., 1981; Naeser et al., 1989). This article will proceed from the assumption that etched track lengths as revealed by the experimental procedures of Green et al. (1986), Duddy et al. (1988), and Donelick (1988) reflect predominantly the kinetics of annealing, whereas the kinetics of chemical etching play a subsidiary role. The best justification for this assumption is the result ultimately extracted from it: the model developed in this article reproduces the kinetics of AFT length reduction in laboratory experiments with an accuracy equal to the precision with which the experimental measurements can be made.

Temperature and time dependence of annealing rates

The predominant controls on rates of AFT annealing are temperature and time; by comparison, effects of track orientation and apatite composition are of smaller magnitude. Consequently, the kinetic model must first address the time and temperature dependence of annealing rates. Toward this end, a physical model of fission-track annealing is developed below, first conceptually, then mathematically. The mathematical model is then verified against the existing data on reduction in mean etchable track length as a function of temperature and time.

Model description of fission-track damage and annealing

If fission tracks consist of disrupted zones laden with defects dominated by vacancies and interstitials, then repair of the disruption can proceed by short translations of atoms (perhaps on the order of ~5–10 Å or less) from abnormal positions into their proper sites in the crystal structure. This atomic repositioning may be similar in many respects to that which takes place during topotactic mineral transformations (cf. Carlson and Rosenfeld, 1981), although the driving force in the case of AFT annealing is the strain energy stored in the disrupted crystal rather than the chemical-potential difference between mineral polymorphs, as in the case of topotactic transformation. As defects are eliminated by these short-range atomic movements, the defect density decreases toward a threshold value that is the minimum density required to produce an appreciable acceleration of dissolution for a given etching procedure. This etching threshold is defined only in terms of the specific techniques used to etch the tracks in a particular laboratory, because a more prolonged or more intense etching process corresponds to a lower effective value for the threshold density. Regions of the crystal in which the defect density drops below this arbitrarily defined etching threshold are "annealed"; regions in which the defect density remains above this threshold are "unannealed." It is clear that variations in etching procedures will affect measurements of annealing kinetics, and such variations are believed to contribute

significantly to the imprecision of available track-length measurements. For the purposes of this article, it is assumed that the attention given by experimentalists to standardization of etching procedures within each laboratory is sufficient to render the etching kinetics a second-order effect, in comparison to the kinetics of track shortening. The experimentally measured rates of AFT annealing are therefore regarded here as depending fundamentally upon (1) the distribution of defects in the crystal surrounding the path of the fission fragments, and (2) the rate at which the defects are eliminated.

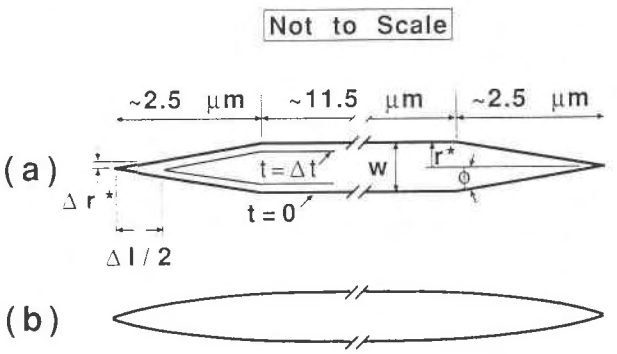

Fig. 1. Schematic representations of disrupted zone in a latent fission track in apatite (not to scale). (**a**) A cylindrical zone of disruption ~11 μm long, with a width w of a few tens of Å, is terminated by two conical tips, each ~2.5 μm in length. The radius of the region that is sufficiently disrupted to etch appreciably faster than the bulk crystal is r^*. As shown on the left, an annealing episode of duration Δt simultaneously produces a decrement of radius (Δr^*) and a decrement of length ($\Delta l/2$ at each end); the ratio of these decrements is the tangent of the taper angle ϕ. (**b**) Alternative representation in which the radius of the disrupted zone decreases monotonically and nonlinearly from the axial center to the tips of the tracks. This geometry yields kinetic predictions that are equivalent, within experimental error, to those produced by the geometry in part (a), but the kinetic equations are mathematically much more cumbersome.

Defect distribution

It is necessary to consider separately the initial axial and radial defect distributions, that is, the distributions in the directions respectively parallel and perpendicular to the path of the fission fragments before any annealing has occurred.

Axial defect distribution. The character of the initial axial defect distribution is suggested by the observation of Green et al. (1986) that, during annealing, tracks shorten systematically from their tips inward toward their centers to about two-thirds of their original length before they abruptly contract and disappear. This observation is consistent with radial shrinkage during annealing of a disrupted zone that is postulated to be nearly cylindrical near its axial center but that tapers near its tips, as illustrated in Figure 1. If the disrupted zone is approximately cylindrical for ~11 μm near its axial center but tapers gradually over an axial length of ~2.5 μm at each end, then radial shrinkage of the disrupted zone will cause a track to shorten to ~11 μm at a rate controlled by the taper angle ϕ (Fig. 1a). The taper angle ϕ is too small for the taper to be evident in HRTEM images: for a disrupted zone 50 Å wide, tapering to a point over a length of 2.5 μm, ϕ is less than $0.001^R = 0.06°$. (To better appreciate the actual shape of such a zone, consider that if a track were enlarged to 100 m in length, it would be only 3 cm wide over a distance of 70 m near its axial center, and the tapering at the track's tips, from a width of 3 cm to a point, would extend over ~15 m at each end.)

This postulated geometry for the disrupted zone requires, during radial shrinkage in the course of annealing, that the radius of the zone near its axial center approaches zero as the length of the zone approaches ~11 μm. Thus, near a length of 11 μm, a change in the dominant mechanism for length reduction is likely, because the track width is close to zero. If there were no variations in defect density axially along the cylindrical portion of the track, the disrupted zone would disappear instantaneously as it reached zero radius simultaneously at all points along its length. But small variations along the track length in defect density or in track diameter might instead cause a track at this juncture to pinch off at random positions along its length, segmenting the track into a number of shorter sections that then segment in turn into still shorter sections, until annealing is complete. Green et al. (1986) alluded to a mechanism of this sort, which is consistent with their detection of unetchable gaps in tracks only in heavily annealed samples. They actually image one instance of etchant breaking through a gap in an annealed sample in their Figure 11 and comment (p. 248) that they observed this phenomenon in about 15% of the tracks they examined in a pair of samples with mean track lengths of 9.7 and 8.8 μm. The onset of a segmentation process when the radius of the disrupted zone nears zero would account for the two characteristic features of the second stage of annealing, namely a very abrupt decrease over time in mean etchable track length and a concomitant marked increase in standard deviations of measured etchable track lengths.

Although the precise geometry of the disrupted zone is largely a matter of conjecture because of the poor constraints available from observation and theory, the simplified geometry presented in Figure 1a is a plausible approximation. As noted in the background section above, a generally cylindrical shape for the disrupted zone is well supported by HRTEM observations and data from small-angle X-ray and neutron scattering. Likewise, the tapering of the zone at its ends is in accord with the theoretical expectation of a decrease toward the end of the zone in the number of defects per unit volume at any chosen radial distance, as the fission fragments' energies decline near the end of their range.

Nevertheless, explicit notice should be taken of the fact that the particular geometry postulated for the disrupted zone shown in Figure 1a has no direct basis in theory or observation. Instead, that geometry has been adopted as

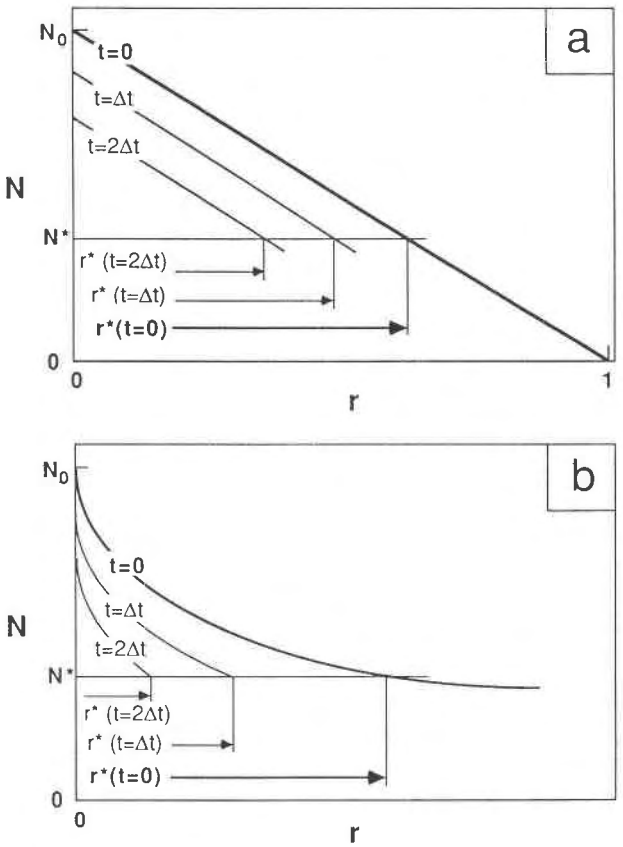

Fig. 2. Possible radial defect distributions (RDDs) in unannealed and isothermally annealed fission tracks. Unlike a linear distribution (**a**), a distribution that is concave upward (**b**) evolves with time in such a way that the radius of the disrupted zone shrinks rapidly at first, but more slowly later. Thus only a distribution that is concave upward is consistent with the decrease of shortening rates over time observed in isothermal annealing experiments.

a simplification, one that is shown in this article to be capable of reproducing the essential features of the annealing process as revealed by the available experiments. Theories for the formation of charged-particle tracks (cf. Fleischer et al., 1975) argue only for a monotonic decrease in the diameter of a fission track away from its axial center. There is no necessity for the diameter of the cylindrical region near the axial center of the disrupted zone to be rigorously constant, and there is likewise no necessity for the diameter of the disrupted zone to change linearly at is tips. Equally plausible is that the taper changes continuously along the length of the latent track, as illustrated in the alternative cross-section through a disrupted zone that appears in Figure 1b. Both alternatives shown in Figure 1 yield kinetic predictions that fall within the precision of presently available experimental measurements, although the geometry of Figure 1b introduces substantially greater mathematical complexity into the kinetic equations. However, if the acceleration of track-shortening rates in the second stage of annealing is real (and not an artifact of the etching process, as some workers have contended) then the model for the kinetics presented here does require an approximately constant diameter for the axially central part of the disrupted zone. If, instead, the acceleration of track-shortening rates in the second stage of annealing is purely an etching artifact, then a double-cone geometry (in which the diameter of the disrupted zone decreases nearly uniformly from the center toward each tip) would suffice to describe the first-stage kinetics, and the central, nearly cylindrical regions in Figures 1a and 1b would not be required.

Radial defect distribution. The character of the initial radial defect distribution (RDD) is revealed by the time dependence of annealing rates in isothermal experimental studies, as follows. The initial RDD must exert fundamental control on the time dependence of the annealing rate, as illustrated in Figure 2, which schematically depicts two initial RDDs and their evolution with time. The vertical axes in that figure correspond to the excess defect density N, defined as the number of defects per unit volume in excess of that for the bulk crystal. The horizontal axes correspond to the fractional radius r, which takes on values ranging from zero at the radial center of the track to unity at the radial distance for which N becomes zero (that is, the distance at which the defect density is equal to that for the bulk crystal). The initial density of defects at the radial center of the disrupted zone is symbolized in Figure 2 by N_0; the threshold value for accelerated etching is designated by N^*; the radial distance at which $N = N^*$ is denoted by r^*, which defines the outermost radius of the region that is sufficiently disrupted to produce appreciably accelerated etching. In Figure 2a, the initial defect density falls off linearly with radial distance, whereas in Figure 2b, the RDD is concave upward so that the defect density drops off much more rapidly with distance at small radii than at large radii.

If one makes the assumption (rationalized below) that the defect-elimination rate at fixed temperature is constant and uniform throughout the crystal, then the density of defects will decrease with time at a rate that is uniform for all values of the radial distance r. This means that with time (at fixed temperature), the RDDs will shift downward at a constant rate, without change of shape, as illustrated by the light lines in Figure 2. As a result, the fractional radius of the disrupted zone (r^*) will decrease as the unannealed region (where $N > N^*$) shrinks toward the radial center of the zone. If the initial RDD were linear as in Figure 2a, then r^* would decrease by equal increments in each unit of time, producing an isothermally time-invariant rate of radial shrinkage; for a constant taper angle, this would likewise produce an isothermally time-invariant rate of track shortening. All experimental data (Green et al., 1986; Duddy et al., 1988; Donelick, 1988) require, however, that rates of axial shortening decrease over time at constant temperature. This necessitates that initial RDDs must be concave upward, as illustrated in Figure 2b. For any initial RDD

that is concave upward, r^* decreases rapidly early in an isothermal annealing event but decreases more slowly later. It will be shown below that an initial RDD with a shape similar to that in Figure 2b (but more strongly curved) generates an isothermal time dependence of annealing rate that accords quantitatively with observation.

This description of the radial defect distribution is consistent in its essential features with the results of small-angle X-ray and neutron scattering studies of Dartyge et al. (1981) and Albrecht et al. (1984, 1985), which approximate the initial RDD with a Gaussian function that is concave upward over all values of r except those very close to the radial center of the track.

Defect-elimination rate

In analogous processes that proceed by short-range atomic repositioning, such as grain boundary migration (Turnbull, 1956) and topotactic transformation (Carlson and Rosenfeld, 1981), the rate of atomic repositioning is constant over time but depends exponentially on temperature. Equivalent kinetics would be reasonable for the closely similar small-scale atomic movements responsible for AFT annealing. Under this analogy, the rate per unit volume at which defects are eliminated by minor atomic repositioning should be uniform throughout the crystal, that is, independent of distance from the radial center of the disrupted zone. Consequently, the defect-elimination rate is expected to be a function of temperature alone, and (in correspondence with the better-understood atomic processes mentioned above) it is expected to increase exponentially with temperature according to the Arrhenius relation, in which the logarithm of the rate varies linearly with inverse absolute temperature.

There is some evidence in the work of Dartyge et al. (1981) that the RDD in some materials may change shape as annealing progresses; this behavior, if it were to occur in apatite, would be inconsistent with a spatially uniform rate of defect elimination. As demonstrated below, however, the postulate of a uniform defect-elimination rate yields excellent agreement with experimental annealing data. Thus any nonuniformities in the defect-elimination rate for apatite and any shape changes of the RDD are negligible at the resolution provided by present experimental measurements.

Kinetic model for axial shortening

In this section, the physical model introduced above for the first stage of annealing is translated into a mathematical form that allows the calculation of annealed track lengths in excess of ~1.1 μm as a function of initial length, time, temperature, and three empirically determined quantities. The symbols used in this article are tabulated and briefly defined in Table 1.

The model seeks to allow calculation of the length l_{as} of a fission track subjected to axial shortening during an annealing event, given its initial length l_0 and its thermal history during the annealing interval Δt. This reduces to a calculation of the corresponding decrement in the fractional radius of the disrupted zone (Δr^*) during the interval Δt, because the geometry of Figure 1 requires that

$$\begin{aligned} l_{as} &= l_0 + \int_0^t \left(\frac{dl}{d\tau}\right) d\tau \\ &= l_0 + \frac{2\left(\frac{w}{2}\right)}{\tan \phi} \int_0^t \left(\frac{dr^*}{d\tau}\right) d\tau \\ &= l_0 + \frac{w}{\tan \phi} \Delta r^*, \end{aligned} \tag{1}$$

in which w is the radial width of the disrupted zone at $t = 0$, and τ is a dummy variable of integration over time. The decrement in the fractional radius of the disrupted zone (Δr^* in Eq. 1) depends upon the defect-elimination rate and the initial radial defect distribution, as described in the two paragraphs that follow.

The defect-elimination rate dN/dt is assumed to obey the equation

$$\frac{dN}{dt} = -c\left(\frac{kT(t)}{h}\right) \exp\left(\frac{-Q}{RT(t)}\right), \tag{2}$$

in which k is Boltzmann's constant; h is Planck's constant; c (>0) is an empirical rate constant; Q (>0) is the activation energy for the atomic motions required to eliminate the defects; R is the universal gas constant; and $T(t)$ is absolute temperature at time t. This defect-elimination rate has no dependence upon radial distance. Equation 2 corresponds closely to the kinetic equation for atomic motions across a coherent interface proposed by Turnbull (1956) and applied to topotactic aragonite-calcite transformation kinetics by Carlson and Rosenfeld (1981). It differs from Turnbull's formulation insofar as it eliminates terms for the reverse reaction, that is, terms for the spontaneous creation of defects by the motion of an atom from a correct site to an interstitial site. The rate of spontaneous creation of defects is thus assumed to be negligible by comparison to the rate of elimination of such defects during thermal annealing.

Although the initial radial defect distribution is not known precisely, its approximate form can be deduced from the experimentally determined dependence of rate upon time in an isothermal anneal. In many experiments, such as those for which results are shown in Figure 3, a linear relation holds between the logarithm of the amount of shortening (Δl) and the logarithm of the isothermal annealing time (Δt). As the derivation in the Appendix shows, that linear relation will arise from any initial RDD that can be approximated by the function

$$N = N_0(1 - r)^{1/n}, \tag{3}$$

in which n is a positive number less than unity. This

TABLE 1. Meaning of symbols

Symbol	Units	Reference equation	Meaning
A	μm	4, A8	Empirical rate constant for axial shortening
b_T	dmnls*	6	Intercept of regression line of ln Δl vs. ln Δt at temperature T
c	dmnls*	2	Empirical rate constant for defect elimination
C	$\mu m \cdot s^{-1}$	A6	Generalized rate constant for isothermal annealing
f	dmnls*	11	Fraction of original track population that has undergone segmentation
h	kcal·s	2	Planck's constant
i	dmnls*	8	Intercept of regression line of b_T vs. $1/T$
k	$kcal \cdot K^{-1}$	2	Boltzmann's constant
l_0	μm	1	Unannealed track length
l_{as}	μm	1, 4	Annealed track length, computed for axial shortening process alone (ignoring segmentation effects)
$l_{as/sg}$	μm	11	Mean track length in population subjected to both axial shortening and segmentation
l_{sg}	μm	13	Track length at which track segmentation becomes appreciable
Δl	μm		Change in track length during annealing interval Δt
m	K	7	Slope of regression line of b_T vs. $1/T$
n	dmnls*	3	Exponent in power-law expression for initial radial defect distribution
N	dmnls*	2, 3	Number of defects per unit volume in excess of bulk crystal
N_0	dmnls*	3	Initial excess defect density at radial center of disrupted zone
N^*	dmnls*	A2	Threshold value of defect density required to accelerate etching
Q	$kcal \cdot mol^{-1}$	2	Activation energy for atomic motions that eliminate defects
R	$kcal \cdot mol^{-1} \cdot K^{-1}$		Universal gas constant
r'	dmnls*	24	Ratio of annealed to unannealed track length
r	dmnls*	3	Fraction of distance from center of disrupted zone to distance at which $N = 0$ (fractional radial distance)
r^*	dmnls*	A2	Fractional radial distance at which $N = N^*$
Δr^*	dmnls*	A3	Change in fractional radius of disrupted zone during annealing interval Δt
s	μm^{-1}	13	Change in f per unit decrement in track length (for $l_{as} < l_{sg}$)
t	s		Time elapsed since beginning of annealing interval
Δt	s		Duration of annealing interval
T	K		Absolute temperature
w	Å	1	Width of disrupted zone prior to annealing
V_{cell}	Å^3	14	Unit-cell volume
V_{ions}	Å^3	14	Total volume of ions in unit cell
Z	dmnls*	14	Total ionic porosity
ϕ	radians	1	Angle of taper of disrupted zone
θ	radians	21	Angle between track and apatite c axis
τ	s		Dummy variable of integration over time

* dmnls = dimensionless quantity.

function has the concave-upward shape required to produce the observed decrease in annealing rate with time at fixed temperature. As n decreases, the degree of curvature increases, and for values of n in the range 0.1–0.3, this function has a shape very similar to the Gaussian curve used by Dartyge et al. (1981) and Albrecht et al. (1984, 1985) to approximate the defect distribution revealed by small-angle X-ray and neutron scattering measurements (Fig. 4). Neither distribution has a theoretical basis; both approximate the actual distribution closely enough to provide useful descriptions of fission-track damage and annealing.

The Appendix details how Equations 1, 2, and 3 can be combined to yield the fundamental relationship between the length of a fission track and its thermal history, namely

$$l_{as} = l_0 - A\left(\frac{k}{h}\right)^n \left[\int_0^t T(\tau)\exp\left(\frac{-Q}{RT(\tau)}\right) d\tau\right]^n, \quad (4)$$

in which l_{as} is etchable length after axial shortening; l_0 is initial (unannealed) length; k is Boltzmann's constant; h is Planck's constant; T is absolute temperature; t is time measured from the beginning of the annealing episode; the three quantities n, Q, and A are empirically determined parameters, with physical significance, that may depend upon apatite composition; and τ is a dummy variable of integration over time. Equation 4 thus describes the length of an annealed fission track in terms of three measurable quantities (initial length, time, and temperature), and three parameters to be determined by experimental measurement: A, a rate constant which incorporates factors for the geometry of a conical track tip and for the defect density at the radial center of the disrupted zone (see Appendix); Q, the activation energy for the atomic motions required to eliminate defects; and n, a number which describes the shape of the initial radial defect distribution via Equation 3.

Verification of the kinetic model for axial shortening

In the case of an isothermal laboratory annealing experiment, Equation 4 takes the form:

$$l_{as} = l_0 - A\left(\frac{kT}{h}\right)^n \exp\left(\frac{-nQ}{RT}\right) t^n. \quad (5)$$

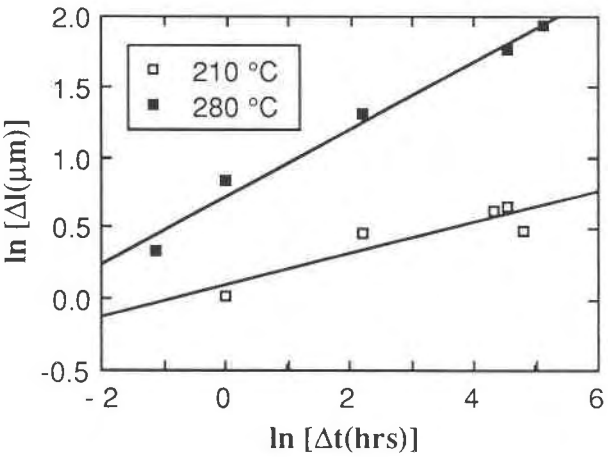

Fig. 3. Plot of experimental data from Green et al. (1986) illustrating a linear relationship between the logarithm of the change of length (Δl) and logarithm of the duration of isothermal annealing episodes (Δt).

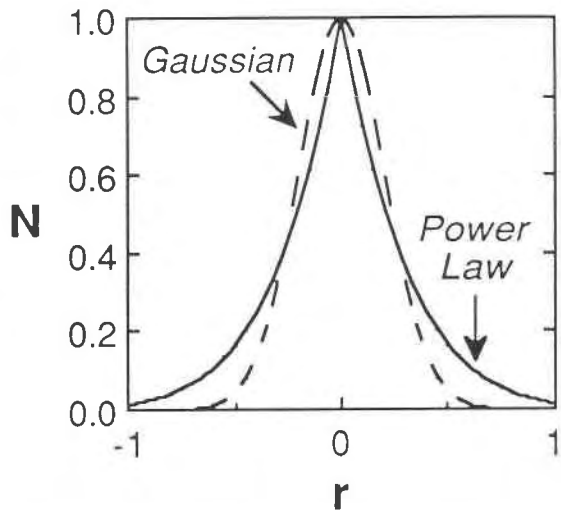

Fig. 4. Comparison of the Gaussian defect distribution (dashed line) used to model small angle X-ray and neutron scattering results (e.g., Dartyge et al., 1981; Albrecht et al., 1984, 1985) with the power-law distribution (solid line) used in this model (Eq. 3, with $n = 0.15$). Neither distribution has a theoretical basis; both approximate the actual distribution closely enough to provide useful descriptions of fission-track damage and annealing.

Equation 5 embodies several predictions for systematic relationships that should be embedded in the experimental annealing measurements at constant temperature. In the following discussion (1) the validity of the model is confirmed by extraction of the predicted relationships from the data; (2) a means of estimating values of n, Q, and A from the data is described; and (3) the predictions of the model for annealed track lengths are tested against available experimental data.

Equation 5 predicts that for annealing experiments yielding lengths as a function of time at constant temperature, linear regression of the logarithm of the change of length (Δl) against the logarithm of the time of anneal (Δt) will produce lines with identical slope (denoted by n) at all temperatures, and intercepts (denoted by b_T) that vary with temperature according to

$$b_T = \ln\left[A\left(\frac{kT}{h}\right)^n\right] + \left(\frac{-nQ}{R}\right)\left(\frac{1}{T}\right). \tag{6}$$

The example in Figure 5 (using the data of Green et al., 1986) illustrates that the predicted relationships are indeed present in the experimental annealing data. Figure 5a shows that values of n obtained from the regression of ln Δl against ln Δt are independent of temperature, although they scatter appreciably. (This variation is equally apparent in the unequal slopes shown in Fig. 3.) Despite the scatter, the mean of several determinations of n provides a good estimate of the best-fit value for n for the data set. Figure 5b shows that the intercepts (b_T) obtained from the regression of ln Δl against ln Δt vary with temperature in a manner consistent with the model's predictions, as follows. Note that in Equation 6, the dependence of b_T on temperature will be dominated by the second term (linear in $1/T$) rather than the first (logarithmic in T^n). Thus, values of b_T should be very nearly linearly related to inverse absolute temperature, so that when values of b_T are plotted on the ordinate against ($1/T$) on the abscissa, linear regression is predicted to produce a slope m and an intercept i given by

$$m = -\frac{nQ}{R}, \tag{7}$$

$$i = \ln\left[A\left(\frac{kT}{h}\right)^n\right]. \tag{8}$$

Again, as the example in Figure 5b illustrates, the data conform to the linear relationship predicted by Equation 6. Although the model actually predicts a slight curvature for data on a plot such as that in Figure 5b, as a consequence of the temperature dependence of the logarithmic term in Equation 6, the curvature is too small to be resolved over small ranges of temperature. Inversion of Equation 7 allows estimation of Q from the relation

$$Q \approx -\frac{mR}{n}. \tag{9}$$

Likewise, an approximate value for A can be obtained by inverting Equation 8, using a temperature value T_{mid} that lies near the middle of the experimental range:

$$A \approx \frac{\exp(i)}{\left(\frac{kT_{mid}}{h}\right)^n}. \tag{10}$$

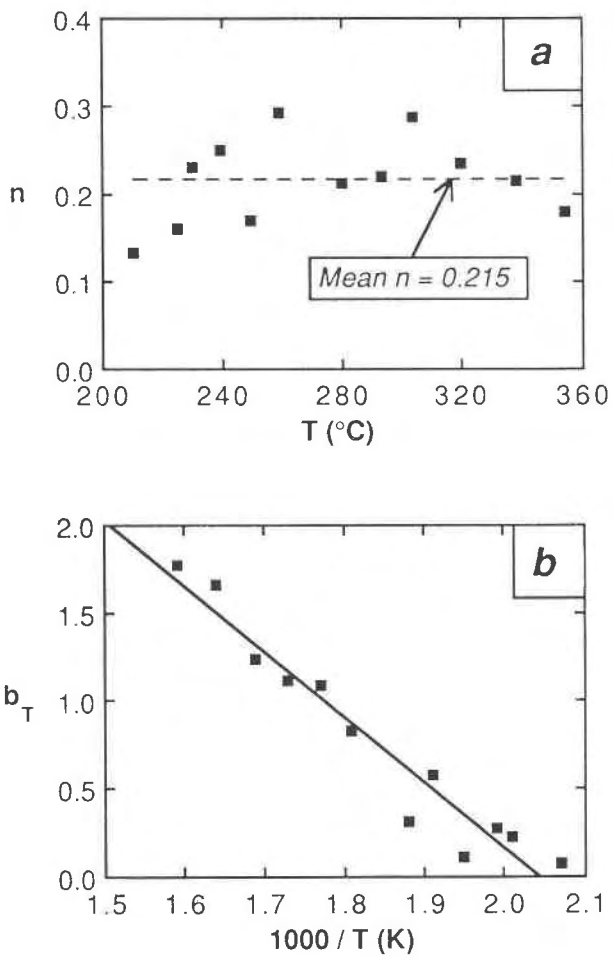

Fig. 5. Confirmation of model predictions for temperature independence of n and temperature dependence of b_T, based on data of Green et al. (1986). (**a**) Values of n extracted from the data show no correlation with temperature, although they scatter by approximately ±50% about their mean. (**b**) Values of b_T extracted from the data are linearly correlated with inverse absolute temperature.

Using estimates for n, Q, and A determined by the procedure outlined above, model lengths of isothermally annealed tracks can be computed from Equation 5 and compared to measured experimental lengths. Agreement is generally good, but because of the scatter apparent in Figures 5a and 5b and the approximations represented by Equations 9 and 10, it is often possible to obtain substantially better fits to the data by means of a least-squares fitting procedure that varies n, Q, and A (in the neighborhood of initial estimates provided by the simple linear fitting procedure), seeking to minimize the discrepancies between measured and modeled lengths. Equation 5 has been fitted to the isothermal annealing data of Green et al. (1986) and Donelick (1988); the best-fit values are listed in Table 2, and comparisons of measured and model lengths appear in Figures 6a and 6b. In addition, the best-fit values for n, Q, and A from the isothermal experiments of Green et al. (1986) have been used in Equation 4 to model the experiments of Duddy et al. (1988), in which temperature varied over time; these results appear in Figure 6c. Because of the change in the mechanism of length reduction in the second stage of annealing, the model requires that populations of tracks with mean lengths less than about 11 μm must shorten more rapidly than Equations 4 and 5 predict. This is indeed the case, as shown by the tendency for points below the short horizontal lines (marking a measured length of 11 μm) to fall to the right of the diagonal. For this reason, those data for which mean measured lengths are less than 11 μm were not included in the fitting procedure used to obtain the values in Table 2. The excellent correspondence in Figure 6 between measured and modeled lengths of experimentally annealed tracks for $l \geq 11$ μm is taken as evidence that the physical model and its mathematical description (Eq. 4) are suitable representations of the first stage in the process of fission-track annealing in apatite.

Table 2. Fitted values of model parameters

Data set*	n	Q (kcal·mol^{-1})	A (μm)
a	0.206	40.6	1.81
b	0.111	49.0	5.85
Composite	0.141	46.5	4.66

* Sources of data: a = Green et al. (1986); b = Donelick (1988).

The best-fit values for n, Q, and A used to produce the correspondence shown in Figure 6 vary about their means by ±30%, ±9%, and ±53%, respectively. Much of this variation is probably unsystematic, because the best-fit values are not rigidly constrained by the data. It is possible to achieve fits to the data that are nearly as good as the best fits by using slightly different values; thus the exact values obtained for these three parameters are largely controlled by a few of the data (often outliers) in each set. In fact, a composite model using $n = 0.141$, $Q = 46.5$ kcal mol^{-1}, and $A = 4.66$ μm replicates nearly all the data for $l \geq 11$ μm, from all three sources, to within the precision with which the experimental measurements can be made (Fig. 7). Considering the differences among studies in materials and in procedures for laboratory annealing, track revelation, and track measurement, the agreement between measured lengths and those calculated by this three-parameter composite model is remarkable.

The fact that the experimental data from all three sources can be fitted using only three empirical parameters is partly a result of the fact that the compositional variation among the experimental apatite samples, especially in the F-Cl ratios, is small. In natural occurrences, Green et al. (1986) and others have inferred substantial differences in annealing rates for apatite of different compositions. A comparison of the best-fit values for n, Q, and A in Table 2 with published compositions suggests that there may be a systematic relationship between values for those parameters and apatite chemistry. If this relationship can be discovered, it should be

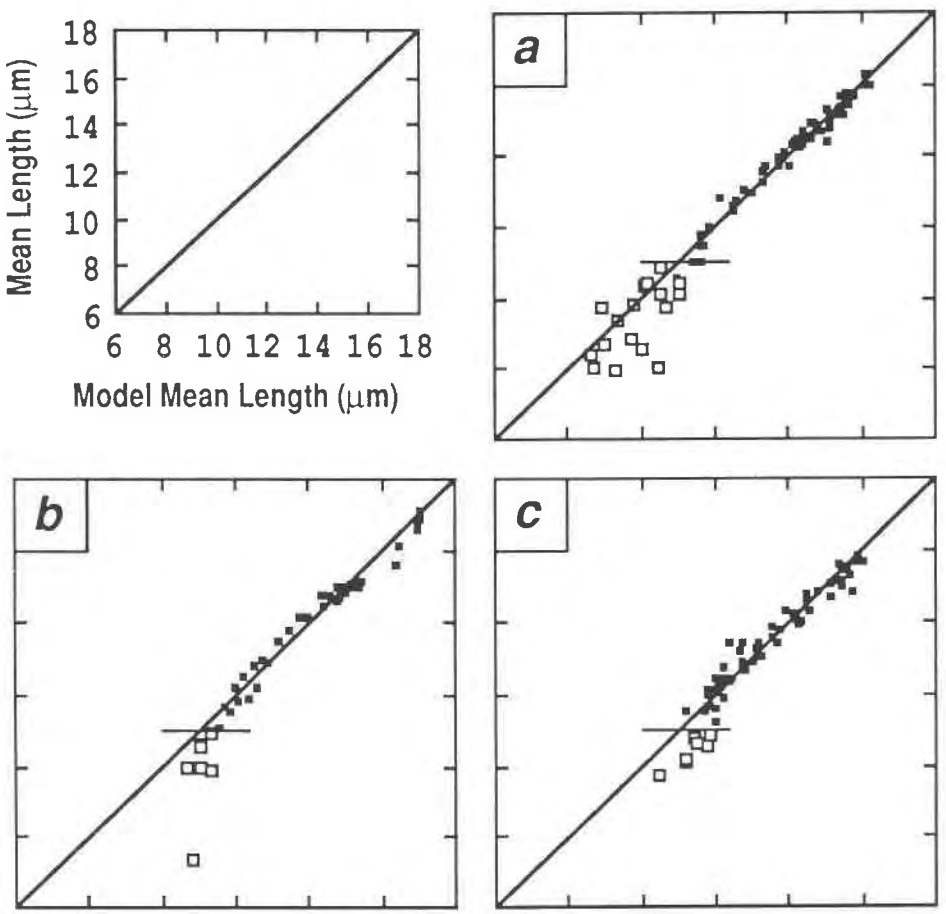

Fig. 6. Comparison of measured mean track lengths and model track lengths calculated from Equations 4 and 5, using parameters for individual samples from Table 2, for experimental data of (**a**) Green et al. (1986); (**b**) Donelick (1988); and (**c**) Duddy et al. (1988). For measured mean lengths greater than 11 μm (filled symbols above short horizontal line), perfect correspondence between the model and experiment would produce points falling on the diagonal line. For measured mean lengths less than 11 μm (open symbols below short horizontal line), the model predicts that calculated lengths should exceed measured lengths, which would produce points falling progressively farther to the right of the diagonal line as measured mean length decreases. Approximate uncertainties in measured mean lengths are indicated in Figure 7.

possible to quantify the compositional dependence of AFT annealing rates. An attempt is made in a subsequent section of this article to identify this relationship on the basis of theoretical considerations and qualitative observations of the relative rates of annealing for apatites of different compositions in experiments and in natural occurrences.

Kinetic model for track segmentation

As described in the background section above, a rapid acceleration in track-length reduction is observed once the track population reaches a mean length of about 11 μm. This was attributed in the foregoing analysis to a change in the predominant length-reduction mechanism, from axial shortening to track segmentation, when the radius of a track's disrupted zone approaches zero. The following discussion presents a simplified quantitative explanation of the track-segmentation process, and an empirical kinetic equation to approximate the reduction in mean length from ~11 μm to the limit of the available data at ~7.5 μm. The model predictions are then tested against the few available experimental data on annealing rates in this second stage and against data on the breadth of the track-length distribution as a function of mean track length.

The track-segmentation process is inherently more difficult to analyze than axial shortening because the rate at which segmentation events occur depends not only upon the defect-elimination rate, but also upon the detailed nature of the core of the disrupted zone after much annealing has taken place. The rate of segmentation is expected to increase exponentially with temperature with the same activation energy as determined above for axial shortening because the individual atomic motions are presumed to be unchanged; only the response of the system in terms of track length is altered. But over time at constant temperature, the rate of segmentation should ac-

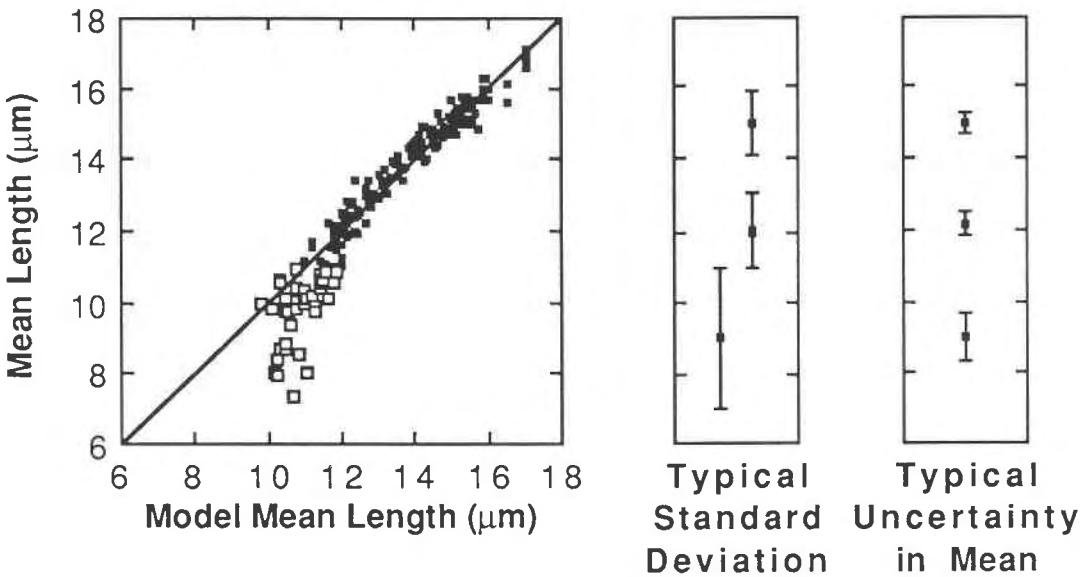

Fig. 7. Comparison of measured mean track lengths and model track lengths calculated from Equations 4 and 5, in which a single set of three parameters (the composite best-fit values in Table 2) are applied to all data sets appearing in Figure 6. Typical standard deviations of measurements are based upon those in Figure 3 of Green et al. (1986). Nominally, uncertainties in means are smaller than the standard deviations by a factor equal to the square root of the number of measurements used to estimate the mean. However, because the imprecision of published replicate measurements is substantially greater than the nominal uncertainty in the mean, the true uncertainty must be larger; the variation in those replicate measurements suggests that the true uncertainties in the means are about one-third of the standard deviation of the measurements, as shown at far right. Lines and symbols have same significance as in Figure 6.

celerate sharply as the radius of the disrupted zone approaches zero because of the rapidly increasing probability of the track healing radially across a narrowing zone of disruption. The complexity and the random character of this process make it difficult to derive an expression for the segmentation rate as an explicit function of time and temperature. Instead, because the likelihood of a segmentation event is most directly related to the radius of the disrupted zone, which is in turn a direct function of the annealed track length, it appears more promising to analyze the segmentation process by seeking in the experimental data a relationship between the mean track length and the amount of segmentation that has occurred.

If a segmentation event interrupts a track of length l at a random position along its length, the track will separate into two sections of lengths x and $l - x$, where x is a random number between zero and l. The mean length of the two resulting sections is $[(l - x) + x]/2$, or exactly half of the original length of the track. Thus a population of annealed tracks that has entered the segmentation stage will consist of two subpopulations, one having a mean length given by Equation 4, and the other with a mean length exactly half as large. Two simplifications are inherent in this statement. First, the statement assumes that the number of original tracks that have undergone more than one segmentation event is negligibly small. This is likely to be true during the early progress of the segmentation process (the only part of the process for which there are experimental data), but it must become less valid as the tracks become nearly obliterated in the final phases of annealing. Second, the above statement assumes that all tracks in a population with a mean length $\lesssim 11$ μm have an equal probability of undergoing segmentation, regardless of their individual lengths or orientations. This assumption simplifies the analysis but neglects the observations of Donelick (1988, p. 141 and Fig. 3.2) and Green et al. (1986, p. 248–249) that suggest preferential segmentation of the shorter tracks at high angles to the c axis. Given the paucity and imprecision of existing experimental measurements at advanced stages of annealing, it is impossible to provide well-constrained alternatives to these assumptions. Thus it is reassuring that the agreement below between experiment and prediction suggests that the errors introduced by these simplifications do not have significant adverse effects on the analysis.

If some fraction f of the original population of tracks has experienced a single segmentation event, then the resulting mean track length of the two subpopulations taken together is given by

$$l_{as/sg} = \frac{[(1 - f)\cdot l_{as}] + \left[2f\cdot\left(\frac{l_{as}}{2}\right)\right]}{(1 - f) + 2f} = \frac{l_{as}}{1 + f}, \quad (11)$$

in which $l_{as/sg}$ designates the mean length of a population of tracks that has undergone both axial shortening and

segmentation, and l_{as} is the mean annealed length resulting from the first-stage axial-shortening process alone, as calculated from Equations 4 or 5. Consequently, estimates of f can be extracted from each of the annealing experiments by inversion of Equation 11 to yield

$$f = \frac{l_{as}}{l_{as/sg}} - 1, \tag{12}$$

in which $l_{as/sg}$ is taken as equivalent to the measured mean track length in the experiment and l_{as} is computed for each experiment from Equations 4 or 5.

Figure 8 shows the variation in f calculated from Equation 12, as a function of $l_{as/sg}$ and of l_{as}, for the experimental data from all three sources. The onset of segmentation at a length $l_{sg} \approx 11$–12 μm is apparent in both diagrams, and both show the expected increase in the fraction of tracks that have been segmented as the mean length decreases. Green et al. (1986, p. 248) reported, for samples annealed for 1 h at 336 and 352 °C with mean track lengths of 9.7 and 8.8 μm, respectively, that 2 of 14 tracks (14%) and 2 of 11 tracks (18%) were observed to have been segmented; these percentages accord well with the fraction of tracks that is predicted to have undergone segmentation on the basis of Equation 12, as shown in Figure 8a.

In the absence of an atomic-scale theory, it is difficult to justify any empirical relationship between the variables more complex than a linear one, despite the slight suggestion of curvature in Figure 8a and the theoretical expectation that the segmentation process should accelerate as the length (and therefore the radius) of the disrupted zone decreases and as multiple segmentation events occur within originally single tracks. The solid line in Figure 8b is thus the best linear fit, passing through zero at $l_{sg} = 12$ μm, to those data for which l_{as} is less than 12 μm. The absolute value of the slope of that line, designated s, is the only parameter required to quantify the track-segmentation kinetics in this empirical approach. Substitution of the quantity $s \cdot (l_{sg} - l_{as})$ for f in Equation 11 yields an expression for the mean track length of populations in which track segmentation is appreciable (that is, in populations with mean lengths less than l_{sg}), namely

$$l_{as/sg} = \frac{l_{as}}{1 + s(l_{sg} - l_{as})}, \quad \text{for } l_{as} \le l_{sg}. \tag{13}$$

Verification of the kinetic model for track segmentation

After evaluating s and l_{sg}, Equation 13 can be combined with Equation 4 to compare the predictions of the segmentation model with observed track lengths in the laboratory experiments that reached advanced stages of annealing. The maximum length l_{sg} for which segmentation has affected an appreciable fraction of the tracks is evidently between approximately 11 and 12 μm: in Figure 8, mean values for f first appear to become nonzero at a length of approximately 12 μm, and are more clearly positive for lengths ≤ 11 μm. Slightly better fits to the data are obtained from larger values of l_{sg}, so a value for l_{sg} of 12 μm was chosen for this comparison. For $l_{sg} = 12$ μm, the best linear fit to the data in Figure 8b yields a value for s of 0.10 μm^{-1}. These values, which determine f, were used with the composite parameters in Table 2 to evaluate mean track lengths for the entire experimental data set from Equations 4 and 13. The resulting agreement between observed and modeled lengths is shown in Figure 9. Although the scatter of points about the line indicating perfect correspondence is greater for track populations that have undergone appreciable segmentation, it does not greatly exceed the uncertainties in the measurements. This is taken as preliminary evidence that the segmentation model is conceptually reasonable.

An independent confirmation of the segmentation

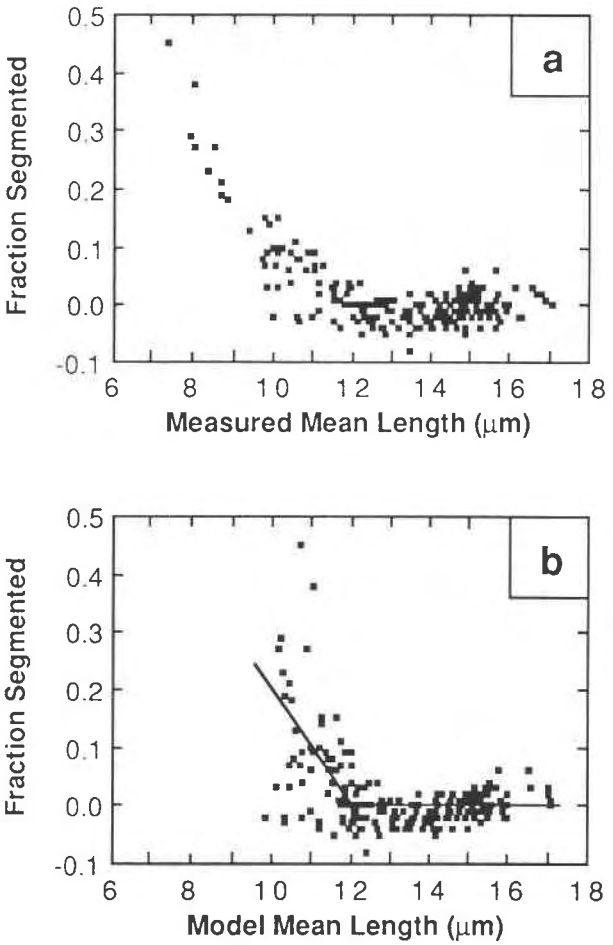

Fig. 8. Fraction of original tracks that have undergone segmentation, computed from Equation 12: (**a**) as function of measured mean track length; and (**b**) as a function of model track length, computed from Equation 4. Solid line is best-fit linear approximation for data with model lengths less than 12 μm.

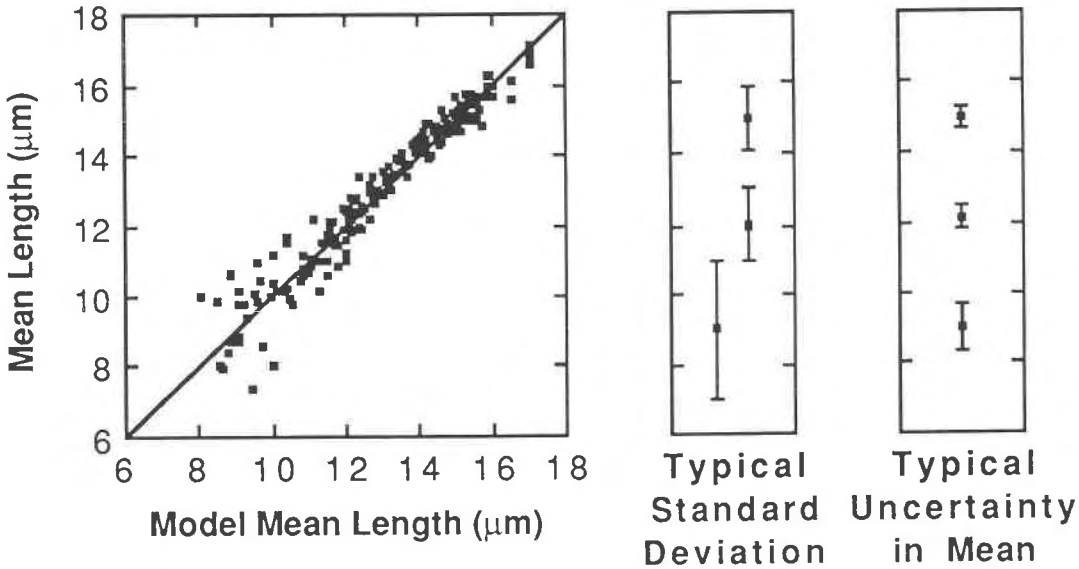

Fig. 9. Comparison, for all isothermal data sets, of measured and modeled mean track lengths. Model track lengths were calculated from Equation 4, using the composite values for n, Q, and A in Table 2, and from Equation 13, using $l_{sg} = 12$ μm and $s = 0.10$ μm^{-1}.

model can be found in the broadening of track-length frequency distributions with increasing degrees of annealing. It is well established that track-length frequency distributions broaden as the mean track length shortens. This is evident in Figure 10, in which standard deviations of experimental track populations as a function of mean track length are plotted. The data in Figure 10 show a gentle rise in the standard deviations as long tracks shorten, followed by an abrupt increase for mean lengths less than about 11 μm. These changes can be explained quantitatively by the present model, which ascribes the initial gradual broadening to the anisotropy of annealing (described below) and the subsequent abrupt broadening to the onset of segmentation.

Changes in the dispersion of the track-length frequency distribution were analyzed by simulating an annealing event for 1000 tracks, whose initial lengths were normally distributed about a mean of 16.5 μm with a standard deviation of 0.8 μm, and whose orientations were randomly distributed with respect to the c axis. At each stage of the simulated annealing process, the length of each track was computed in accordance with Equations 4, 19, and 20 (below), and the mean and standard deviation of the track lengths were evaluated. In track populations for which the mean length resulting from the axial shortening process (l_{as}) was less than l_{sg}, some of the tracks (a fraction of the total given by $[s\cdot(l_{sg} - l_{as})]$) were then subjected to a segmentation event. The tracks to be segmented were chosen at random; each was separated into two segments at a random position along its length. The mean and standard deviation of the track population were then recalculated. The simulation used values of n, Q, and A for the composite data set (Table 2). Assignment of the values for l_{sg} and s involved some ambiguity. It appears in Figure 10 that the length at which the abrupt broadening of the frequency distribution occurs may be as small as 10 μm in some experiments and nearly as large as 12 μm in others. It is quite possible that this quantity varies from experiment to experiment as a function of apatite composition, etching procedure, or other unidentified natural or experimental factors. For the purposes of this comparison, a value of 11 μm was chosen for l_{sg}; reference to Figure 8b suggested a corresponding value of 0.15 for s. To account for the low probability of revelation and observation of very short tracks, segments with lengths <2 μm were not included in the calculation of means and standard deviations.

The results of this simulation are shown as the solid lines in Figure 10, superimposed upon the measured values. The model produces excellent correspondence for track lengths greater than 11 μm, for which the only contribution to the dispersion is the anisotropy of the annealing kinetics (explored more thoroughly in a section below that describes the orientational dependence of annealing rates). Figure 10 also provides evidence for the operation in the later stages of annealing of a segmentation mechanism like that hypothesized above, because it accounts, at least qualitatively, for the abrupt increase in measured standard deviations for tracks shorter than ~11 μm. Additional data on track populations that have reached this advanced stage of annealing will be required to produce more precise quantification of this process.

Compositional dependence of annealing rates

The physical model presented above suggests an approach to the problem of the compositional dependence of AFT annealing rates that exploits the similarity be-

tween the mechanism of O diffusion in silicates and the mechanism of atomic repositioning postulated for AFT annealing. Fortier and Giletti (1989) have shown that rates of O diffusion in many silicates can be described by a single equation that modifies the typical Arrhenius relation for the O diffusion coefficient with additional terms accounting for structural variation. The structural effects are encapsulated in a single quantity Z, called the total ionic porosity, defined by

$$Z \equiv 100 \cdot \left[\frac{V_{\text{cell}} - V_{\text{ions}}}{V_{\text{cell}}} \right], \tag{14}$$

in which V_{cell} is the unit cell volume and V_{ions} is the total volume of ions in the unit cell. The total ionic porosity is thus the percentage of the volume of a unit cell not occupied by the ions themselves; it can be calculated directly from a knowledge of the crystal structure, the crystal composition, the ionic radii in a hard-sphere approximation, and an estimate of the variation of unit-cell volume with composition. Because diffusion and other types of atomic repositioning require the motion of ions past one another, higher values of the total ionic porosity might be expected to permit more rapid repositioning. This is indeed found to be the case for the diffusion of O (and Ar) in silicates under hydrothermal conditions. Except for the highly anisotropic sheet silicates, the following equation of Fortier and Giletti (1989) (in which α, β, γ, and δ are single-valued, empirically determined constants) is capable of reproducing values of the diffusion coefficient D for O in silicates to within about a factor of two:

$$\log D = \alpha + \left(\frac{\beta}{T}\right) + \left(\gamma + \frac{\delta}{T}\right) Z. \tag{15}$$

When this equation is recast as

$$\log D = (\alpha + \gamma Z) + (\beta + \delta Z)\left(\frac{1}{T}\right) \tag{16}$$

it becomes clear that in the case of O diffusion in silicates, both the logarithm of the preexponential rate constant and the activation energy for diffusion are linearly dependent upon the total ionic porosity.

The analogy with AFT annealing may be direct insofar as similar mechanisms of atomic repositioning are involved. It is possible, therefore, that the logarithm of the preexponential constant A and the activation energy Q for AFT annealing are linearly dependent upon the total ionic porosity of the apatite; the parameter n, which describes the initial radial defect distribution surrounding the path of the fission fragments, might also show such a dependence upon composition. At present, however, it is premature to correlate best-fit values of n, Q, and A with Z on the basis of published experimental data sets, because of the low sensitivity of the fits in Figure 6 to small

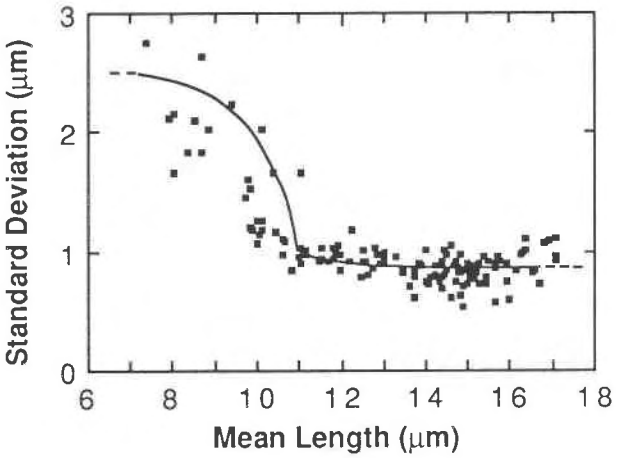

Fig. 10. Comparison of observed broadening of track-length frequency distribution (dots, from isothermal data sets in Table 2) with predictions of model (lines). The small increase in the standard deviation for $l > 11$ μm is solely the result of the anisotropy of annealing rates, whereas the pronounced increase for $l < 11$ μm is the consequence of the onset of segmentation, with relatively minor contributions from annealing anisotropy.

variations in the values of the parameters and because data are presently available for only two compositions, spanning a narrow range of total ionic porosity. Until experimental data on a wider range of compositions become available, support for this explanation of the compositional dependence of annealing rates must be sought instead in qualitative observations of relative annealing rates.

Table 3 affords a comparison of estimated values of Z for the two experimental materials and for three Ca endmember apatite compositions. The most significant reduction in Z is produced by increasing Cl content, in agreement with the qualitative observations of Green et al. (1985) and others that large values of Cl-F in apatite exert the strongest inhibiting effect on annealing in nature. The effects of Cl in place of F and of OH in place of F are also in agreement with the qualitative experimental results reported by Crowley and Cameron (1987). Thus, despite the paucity of data, the outcome of this analysis is encouraging insofar as model predictions of variation in AFT annealing rates with total ionic porosity are of the correct sign and approximately the correct magnitude to account for the observed differences in annealing rates.

The idea that A, Q, and perhaps n may be linearly dependent on total ionic porosity is put forward here as a testable hypothesis that is consistent with present knowledge. Caution is in order: this approach to the compositional dependence of AFT annealing rates cannot be validated until additional experimental data spanning a wider range of compositions are available. Nevertheless, an attempt to identify a relationship between annealing rate and total ionic porosity (or another similar measure of the closeness of packing of atoms in an apatite crystal)

TABLE 3. Idealized compositions and calculated total ionic porosities

	Experimental compositions*		End-member compositions		
	a	b	Ca-OH	Ca-F	Ca-Cl
Ca	4.99	5.00	5	5	5
Sr	0.01	0	0	0	0
OH	0	0.23	1	0	0
F	0.92	0.65	0	1	0
Cl	0.08	0.12	0	0	1
a (Å)	9.3973	9.4153	9.4121	9.3773	9.6269
c (Å)	6.8782	6.8706	6.8773	6.8884	6.7613
a/*c*	1.37	1.37	1.37	1.36	1.42
Z	37.000	36.859	37.334	37.303	33.631
$Z - Z_{Ca\text{-}F}$	−0.304	−0.445	+0.030	0	−3.672

Note: Values of *Z* are calculated using radii (in Å) from Shannon (1976) for [9]Ca (1.18), [7]Ca (1.06), [7]Sr (1.21), [4]P (0.17), [3]O (1.36), [3]OH (1.34), [3]F (1.30), and [6]Cl (1.81); substitutions of other ions are disregarded. Unit-cell edge lengths are calculated as linear combinations of end-member values (i.e., ignoring Sr substitution), which are chosen to give agreement with the measured near end-member values of Hughes et al. (1989).

* Sources of data: a = Green et al. (1986), Young et al. (1969); b = Donelick (1988 and personal communication).

may be a fruitful first step toward constraining the compositional dependence of rates of thermal annealing.

Orientational dependence of annealing rates

Many investigators have noted that the etched lengths of partially annealed fission tracks parallel to the **c** axis are systematically longer than those of tracks perpendicular to the **c** axis in the same crystal (e.g., Green and Durrani, 1977; Green, 1981; Laslett et al., 1982; Donelick, 1988). The following discussion demonstrates that this anisotropy of annealing can be readily explained in the context of the present model by invoking relatively small differences in the widths or taper angles (or both) of disrupted zones in different crystallographic orientations.

Observations

Donelick (1988) measured mean etched lengths of tracks both parallel and perpendicular to the **c** axis in sets of isothermal annealing experiments and drew the following conclusions. (1) Although small differences in etched lengths of unannealed tracks are dominantly the result of unequal rates of bulk etching operating on latent tracks of equal or nearly equal length, the more marked differences in etched lengths of annealed tracks are the consequence of anisotropic annealing (p. 115). (2) Annealed track lengths are an elliptical function of the angle θ between the track and the crystallographic **c** axis (p. 27), and the differences in annealed track lengths for various orientations become increasingly pronounced with increasing degrees of annealing (p. 48). At advanced stages of annealing, the elliptical relation breaks down because tracks nearly perpendicular to the **c** axis enter the second, accelerated, stage of annealing sooner than those nearly parallel to the **c** axis (p. 141). (3) The activation energy for annealing has a negligible dependence upon track orientation (p. 157; see also Ravenhurst et al., 1989).

Figure 11 illustrates an additional conclusion that can be drawn from Donelick's (1988) data: the ratio between the length reduction for tracks perpendicular to the **c** axis and that for tracks parallel to the **c** axis is a nearly constant value, independent of the degree of annealing as indexed by the conventional mean track length. Averaged over all of Donelick's experiments with conventional mean lengths in excess of 11 μm, that ratio is 1.3, with a standard deviation of 0.1. (Although there appears to be a slight tendency for shorter tracks to have higher length-reduction ratios, the slope of a linear regression through the data is not significantly different from zero in a statistical sense, because of the relatively large uncertainties that characterize the experimental measurements.)

Relationship of observations to present model

The model developed in this article is in accord with Donelick's (1988) inference that the anisotropy of annealing is not a consequence of orientational variations in activation energy. The activation energy Q associated with the annealing process in the present model is a macroscopic mean quantity, independent of the actual direction of the atomic displacements involved, independent of the track orientation, and independent of the degree of annealing.

The constant ratio of 1.3 between the length reduction for tracks perpendicular to the **c** axis and that for tracks parallel to the **c** axis (Fig. 11) has an important implication: the anisotropy of annealing probably does not reflect substantial differences in the radial defect distribution for tracks in different orientations, but more likely reflects anisotropy in the width and taper angles of the disrupted zones. This is made evident by expressing the relevant ratio in terms of the fundamental annealing rate law (Eq. 4), placing subscripts on the parameters A, w, ϕ, and n to indicate the possibility of anisotropy in their values and abbreviating the thermal history integral and its preceding frequency factor as '$fcn[T, t]$':

$$\frac{l_{0,\perp} - l_{as,\perp}}{l_{0,\parallel} - l_{as,\parallel}} = \frac{A_\perp \cdot fcn[T, t]^{n_\perp}}{A_\parallel \cdot fcn[T, t]^{n_\parallel}} = \frac{w_\perp}{w_\parallel} \cdot \frac{\tan \phi_\parallel}{\tan \phi_\perp} \cdot \left[fcn(T, t)\right]^{n_\perp - n_\parallel}. \quad (17)$$

If the exponent $(n_\perp - n_\parallel)$ of the thermal history integral ($fcn\,[T, t]$) were appreciably different from zero (i.e., if $n_\perp \neq n_\parallel$), then the rightmost factor in Equation 17 would take on different values for different thermal histories and different degrees of annealing, contradicting the observation of a nearly constant value as indicated by the data in Figure 11. This implies that the value of n, which characterizes the radial defect distribution, is sensibly independent of track orientation.

Because neither the activation energy (Q) nor the radial defect distribution (characterized by n) exhibits orienta-

tional anisotropy, the anisotropy of annealing rates must result instead from variations in the factors affecting the third model parameter (A). Anisotropic variations in A would follow directly from differences in the the geometry of the disrupted zones for tracks in different crystallographic orientations. Evaluation of Equation 17 indicates that the geometric differences required to produce length reductions in the ratio 1.3/1 are small. If one assumes a single zone width of 50 Å diminishing to zero over a mean distance of 2.5 μm, then the required taper angles of the disrupted zones parallel and perpendicular to the c axis would be $0.0012^R = 0.066°$ and $0.0009^R = 0.051°$, respectively. Conversely, if one assumes a single taper angle and a mean width for the disrupted zones of 50 Å, then the required initial radii of disrupted zones parallel and perpendicular to the c axis would be 44 Å and 56 Å, respectively. Regardless of whether the anisotropy is ascribed to widths or to taper angles of disrupted zones, or to both (the most probable choice), the model can explain the observed anisotropy of length reduction by invoking slight differences in the geometry of the disrupted zone that lead to the relationship

$$\frac{A_\perp}{A_\parallel} = 1.3 \tag{18}$$

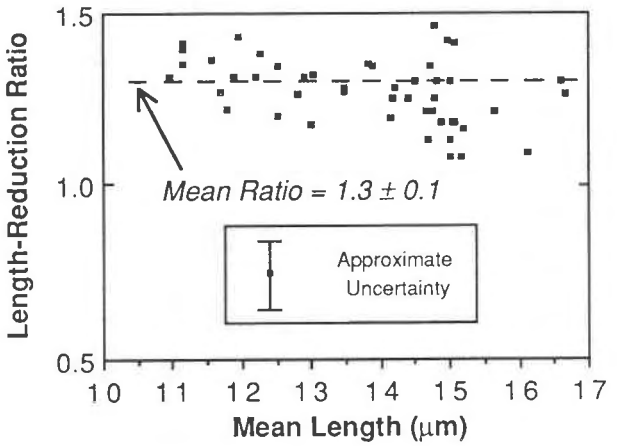

Fig. 11. The quantity $(l_{0,\perp} - l_{as,\perp})/(l_{0,\parallel} - l_{as,\parallel})$ as a function of conventional mean length. The invariance of this ratio over a range of thermal histories signifies that anisotropic variation in the radial defect distribution is negligible, as explained in the text.

Extension to tracks in arbitrary orientation

The dependence of annealing rates on orientation in this model arises solely from anisotropy in the geometry of the disrupted zone, which must in turn result solely from the crystallographic spacing of atoms in the apatite structure. The physical explanation for the elliptical variation in the anisotropy of annealing observed by Donelick (1988) lies in this direct dependence of the annealing-rate constant on the crystal structure of apatite. Because the crystallographic spacing is a property of the crystal structure governed by a symmetrical second-rank tensor, the dependence of the annealing-rate constant upon direction can be described by a ellipsoidal representation quadric (cf. Nye, 1957, p. 17), of which a more familiar example is the optical indicatrix. In other words, the uniaxial symmetry of the apatite structure ensures that the annealing-rate constant varies elliptically between a maximum $A_\perp$ for tracks perpendicular to the c axis ($\theta = \pi/2$) and a minimum $A_\parallel$ for tracks parallel to the c axis ($\theta = 0$). Specifically, the annealing-rate constant for a track in a direction making an angle θ with the c axis is the radius at angle θ of an ellipse (defining the rate constant as a function of track direction) with principal semimajor axes $A_\perp$ and $A_\parallel$. The rate constant is thus given by

$$A_\theta = \sqrt{\frac{A_\parallel^2 \cdot (1.3A_\parallel)^2}{A_\parallel^2 \sin^2\theta + (1.3A_\parallel)^2 \cos^2\theta}}. \tag{19}$$

If track orientations are distributed randomly with respect to the direction of the c axis, then the mean annealing-rate constant averaged over all orientations (A_{mean}) will be the mean radius of the ellipse, that is,

$$A_{mean} = \frac{2}{\pi}\int_0^{\pi/2} A_\theta \, d\theta = 1.135A_\parallel = \frac{1.135}{1.3}A_\perp, \tag{20}$$

in which the integral has been evaluated numerically.

According to the model, rates of length reduction are directly proportional to the rate constant A; thus annealing rates (dl/dt) will vary with orientation in exactly the same way that the rate constant does, as specified by Equations 18, 19, and 20. Consequently, the annealing rate of a track in any arbitrary orientation can be computed from the mean annealing rate by using a pair of equations identical to Equations 19 and 20 but with the quantity (dl/dt) inserted in place of A. Also, to the extent that conventional mean-length measurements sample, with truly equal probability, tracks in all orientations relative to the c axis, the conventional mean length of annealed tracks is related to lengths of annealed tracks parallel and perpendicular to the c axis by substitutions of

$$\left(\frac{dl}{dt}\right)_{mean} = 1.135\left(\frac{dl}{dt}\right)_\parallel = \frac{1.135}{1.3}\left(\frac{dl}{dt}\right)_\perp \tag{21}$$

into the integrand of Equation 1. Conventional mean lengths, however, may be biased by preferential measurement of more highly visible tracks perpendicular to the c axis, and by preferential revelation of longer tracks parallel to the c axis (cf. Laslett et al., 1982). Thus, in the analysis of natural or experimental data in which orientational anisotropy of annealing may play an important role, it is probably advisable to record both track length and orientation, and use the relation in Equation 19, with the quantity (dl/dt) inserted in place of A, to convert all measurements to a uniform reference orientation.

The value of 1.3 ± 0.1 for the annealing-rate ratio obtained from Donelick's experiments is expected to show only slight variation with apatite composition, because it is a direct function of the anisotropy of the crystal structure of apatite. The ratio of unit-cell edge lengths (a/c) provides a crude index of the degree of anisotropy of an apatite structure; the data in Table 2 show variations in (a/c) for the three compositional end-members of only about 2%. Insofar as this relative variability is less than the experimental uncertainty of about 15% in the annealing-rate ratio, a value of 1.3 is probably appropriate for all apatite compositions.

Verification of model against experimental data

An independent validation of the orientational dependence of the model is found in Figure 10. In the course of the simulation described above (in the section verifying the model for track segmentation), track orientations were assigned randomly, and the annealing of each track was computed using the composite value for A_{mean} in Table 2 and the relationships expressed in Equations 19 and 20. The calculated gentle increase in standard deviations before the onset of segmentation (solid line in Fig. 10 for $l > 11$ μm) is in good agreement with the increase observed in the experiments. In the absence of segmentation, that gentle increase is calculated to continue to shorter mean lengths. Thus the abrupt increase for $l <$ 11 μm cannot be ascribed to the effects of annealing anisotropy [one of the two factors invoked by Green et al. (1986, p. 249)]; it should instead be regarded as evidence in favor of the operation of a kinetically distinct segmentation mechanism that becomes dominant in advanced stages of annealing.

It is apparent from the simulation performed here that the anisotropy of annealing, while critical to the proper analysis of experimental annealing data, is nevertheless a comparatively unimportant factor among those that affect natural track-length frequency distributions. By comparison to the initial variation in track lengths and the variability resulting from the continuous production of tracks throughout the thermal history of a natural apatite crystal, the broadening of the frequency distribution that results from more rapid annealing of tracks perpendicular to the c axis is a relatively insignificant agent. The effects of anisotropy may become more substantial when the annealing process enters the second (accelerated) stage, because the observations of Donelick (1988) and Green et al. (1986) suggest that tracks perpendicular to the c axis are the first to undergo segmentation. For those geologic applications in which segmentation is not appreciable, it is probably sufficient to treat track populations solely in terms of their mean lengths, without regard for the effects of anisotropy. When the geologic application demands more precise analysis, it is of course possible to account explicitly for orientational variations in annealing rates by measuring the orientation of each track and using the relationship in Equation 19 to evaluate the annealing rate for each track individually.

Relationship to previous models

The present mechanistic model exhibits significant differences from previous empirical approaches: unlike its predecessors, this model addresses both the orientational and compositional dependence of annealing rates and provides a rate equation sufficiently general to accommodate any arbitrary thermal history; moreover, it is distinct in its explicit recognition of two kinetically distinct stages of annealing, reflecting grossly dissimilar mechanisms of length reduction. If disparate mechanisms do operate at different stages of the annealing process, then any attempt to describe the entire annealing process with a single kinetic equation will inevitably misrepresent the kinetics of one or the other of the stages, or will arrive at an intermediate expression that compromises both to some degree.

The following discussion demonstrates that the present kinetic equations, derived from the physical mechanisms proposed above, include the empirical parallel model of Laslett et al. (1987) as a special case. It also suggests that the differences that arise between the present model and the fanning model of Laslett et al. (1987) are the consequence of the use in the fanning model of a single mathematical formalism to describe two kinetically dissimilar processes.

Comparison with the parallel model

Laslett et al. (1987) present an empirical model that produces parallel contours of equivalent length reduction on a plot of the logarithm of annealing time against inverse absolute temperature (the "parallel Arrhenius plot"). That model, given by their Equation 14, is directly applicable only to an isothermal anneal. It has the form

$$\ln(1 - r') = 3.87 + 0.219(\ln t - 19270T^{-1}) \quad (22)$$

in which r' is defined as the ratio of the annealed to the unannealed length of the track ($r' \equiv l/l_0$). The kinetic model in this article, when reduced to the isothermal form of Equation 5 and when restricted to the axial-shortening stage of annealing, differs from the above expression only by a small temperature factor (T^n, arising from the characteristic vibrational frequency factor in Eq. 2). This can be seen by recasting Equation 5 in the form

$$\ln(1 - r') = \ln\left(\frac{A}{l_0}\right) + n \ln\left(\frac{kT}{h}\right) + n\left(\ln t - \frac{Q}{R}T^{-1}\right). \quad (23)$$

The sum of the first two terms on the right side of Equation 23 varies by less than ±1% over the temperature range 100–300 °C, so it is not surprising that an empirical fit to the data does not reveal this slight temperature dependence. When that dependence is ignored, Equation 5 of this article, derived for an isothermal anneal directly from the physical model, becomes equivalent to the em-

pirical parallel model of Laslett et al. (1987). The present mechanistic treatment therefore provides a physical interpretation for empirical equations of this type.

The near equivalence of the two models results, of course, from the fact that the present model approximates the initial radial defect distribution by the power-law function of Equation 3, which was chosen specifically to yield the logarithmic time-dependence evident in Figure 3. It is this same logarithmic dependence that dominates the empirical fit to the data in the model of Laslett et al. (1987). If the present model had instead adopted a Gaussian function for the initial RDD, it would have generated a more complex expression for the length of an annealed track, with a markedly different mathematical appearance, but that formalism would nevertheless produce quite similar calculated track lengths.

The values of the parameters fitted in this article to the data of Green et al. (1986) differ slightly from those obtained by Laslett et al. (1987) from the same data, reflecting the exclusion in the present case of those experiments that have been appreciably affected by track segmentation. This underscores the importance of accounting explicitly for the change in the dominant mechanism of length reduction as annealing progresses to more advanced stages.

Comparison to the fanning model

In an attempt to refine their parallel model to produce a better fit to the experimental data in the range $r' < \sim 0.65$ ($l < \sim 11$ μm), Laslett et al. (1987) developed a more complex, five-parameter model that produces slightly divergent contours of equal length reduction (the "fanning Arrhenius plot"). Although the fanning model accounts for 98.0% of the variation in the length data, as contrasted with 96.7% for the parallel model, the originators of the model acknowledge that the fanning may be only an artifact, arising from "superposition of competing processes" (Duddy et al., 1988, p. 29).

The physical model presented here suggests that the fanning, which results from modifications required to fit the data at lengths less than ~ 11 μm, probably reflects a change in the predominant mechanism of length reduction for short tracks, as track segmentation becomes more significant than axial shortening. The acceleration in length reduction that arises from the onset of track segmentation produces inflections of the contours of equal length reduction that correspond to those of the fanning model.

Variable-temperature annealing histories

An especially important practical difference between this model and each of the empirical models of Laslett et al. (1987) is its more general nature. The questions of whether or not empirical equations derived from isothermal experiments can be utilized to analyze more complex thermal histories and how this can be done have plagued previous approaches to geologic applications of experimental annealing data. In practice, variable-temperature histories have been treated in earlier work by invoking the concept of equivalent time (Goswami et al., 1984; Duddy et al., 1988). This difficulty does not arise in the case of the present model because of its explicitly polythermal formalism. As presented in Equation 4, the fundamental kinetic equation is directly integrable by numerical means for any arbitrary thermal history; an isothermal history is merely a special case among more general possibilities. In the context of this physical model, it becomes evident that the successive recalculations of equivalent time employed by Duddy et al. (1988) to treat non-isothermal annealing are in fact a coarse approximation to a numerical evaluation of the time-temperature integral that appears in Equation 4.

Conclusions

The fundamental controls on the annealing of fission tracks in apatite are the initial axial and radial distributions of crystalline defects, and the rate at which those defects are eliminated. Within the limits of present experimental and observational evidence, the axial defect distribution can be approximated by a zone of disruption that is cylindrical near its axial center but that tapers at both ends, and the radial defect distribution can be approximated by a power-law function that concentrates defects strongly near the radial center of the zone. Defects are eliminated by short-range atomic repositioning, at rates that can be treated as independent of time and spatially uniform, but that depend exponentially upon temperature. Present evidence suggests that the annealing process encompasses two kinetically distinct mechanisms. Axial shortening is predominant in track populations with mean lengths greater than about 11 μm; at shorter mean lengths, track segmentation is predominant.

Kinetic equations derived from this physical model predict the time and temperature dependence of annealing rates in quantitative agreement with laboratory experiments, for both the axial-shortening and the track-segmentation stages of annealing. The physical model leads to a testable hypothesis for the effect on annealing rate of apatite composition: rate constants, activation energies, and perhaps defect distributions may depend directly upon total ionic porosity, in agreement with qualitative inferences from sparse existing data. The physical model also provides a reasonable explanation for the effect on annealing rate of track orientation. It provides a quantitative explanation for both the gradual and the abrupt broadening of track-length frequency distributions with progressive annealing, as the respective consequences of annealing anisotropy and the onset of track segmentation. When restricted to isothermal annealing in the axial-shortening stage, the equation for the kinetics of length reduction derived from the physical model is closely similar to the parallel model of Laslett et al. (1987). More elaborate models invoking a variable activation energy may reflect inaccuracies introduced by attempts to use a single equation to describe two kinetically dissimilar processes of length reduction. The kinetics of apatite fission-track annealing are presented here in a form that

is numerically integrable over any arbitrary thermal history, obviating the need for the concept of equivalent time.

In all likelihood, more sophisticated observations will encourage more realistic and more comprehensive models for the axial and radial defect distributions in latent tracks, and more extensive experimentation will certainly allow further refinement of values for the critical kinetic parameters. The most significant contribution of this article, therefore, is likely to be its demonstration that by specifying the defect distribution in a latent track and the rate at which defects are eliminated during annealing, it is possible to predict the annealing kinetics for latent tracks possessing defect structures of arbitrary complexity.

Acknowledgments

Special gratitude is expressed to Kevin Crowley, Maryellen Cameron, and Ray Donelick for providing preprints of papers in press. Leslie White brought the problem of fission-track annealing kinetics to my attention and contributed valuable ideas concerning the orientational dependence of annealing rates. Mark Cloos and Jeff Corrigan helped to refine the ideas in this paper over the course of several discussions. I am particularly grateful for penetrating critical reviews of the original manuscript by Kevin Crowley, Ray Donelick, and John Hughes, each of whom pointed out important misconceptions, indeterminacies, or omissions. The Geology Foundation of the University of Texas helped to defray the costs of publication.

References Cited

Albrecht, D., Armbruster, P., Spohr, R., Roth, M., Schaupert, K., Stuhrmann, H. (1984) Small angle scattering from oriented latent nuclear tracks. Nuclear Instruments and Methods in Physics Research, B2, 702–705.

——— (1985) Investigation of heavy ion produced defect structures in insulators by small angle scattering. Applied Physics, A37, 37–46.

Carlson, W.D., and Rosenfeld, J.L. (1981) Optical determination of topotactic aragonite-calcite growth kinetics: Metamorphic implications. Journal of Geology, 89, 615–638.

Chadderton, L.T. (1988) On the anatomy of a fission fragment track. Nuclear Tracks and Radiation Measurements, 15, 11–29.

Chadderton, L.T., Biersack, J.P., and Koul, S.L. (1988) Discontinuous fission tracks in crystalline detectors. Nuclear Tracks and Radiation Measurements, 15, 31–40.

Crowley, K.D., and Cameron, M. (1987) Annealing of etchable fission-track damage in apatite: Effects of anion chemistry. Geological Society of America Abstracts with Programs, 19, 631–632.

Dartyge, E., Duraud, J.P., Langevin, Y., and Maurette, M. (1981) New model of nuclear particle tracks in dielectric minerals. Physical Review B, 23, 5213–5229.

Donelick, R.A. (1988) Etchable fission track length reduction in apatite: Experimental observations, theory, and geological applications. Ph.D. dissertation, Rensselaer Polytechnic Institute, 414 pp.

Duddy, I.R., Green, P.F., and Laslett, G.M. (1988) Thermal annealing of fission tracks in apatite. 3. Variable temperature behaviour. Chemical Geology (Isotope Geoscience Section), 73, 25–38.

Fleischer, R.L., Price, P.B., and Walker, R.M. (1975) Nuclear tracks in solids. University of California Press, Berkeley, 605 p.

Fortier, S.M., and Giletti, B.J. (1989) An empirical model for predicting diffusion coefficients in silicate minerals. Science, 245, 1481–1484.

Fuchs, G., Studer, F., Balanzat, E., Groult, D., Toulemonde, M., and Jousset, J.C. (1987) Influence of the electronic stopping power on the damage rate of yttrium-iron garnets irradiated by high-energy heavy ions. Europhysics Letters, 3, 321–326.

Goswami, J.N., Jha, R., and Lal, D. (1984) Quantitative treatment of annealing of charged particle tracks in common rock minerals. Earth and Planetary Science Letters, 71, 120–128.

Green, P.F. (1981) "Track-in-track" length measurements in annealed apatites. Nuclear Tracks and Radiation Measurements, 5, 121–128.

Green, P.F., and Durrani, S.A. (1977) Annealing studies of tracks in crystals. Nuclear Tracks and Radiation Measurements, 1, 33–39.

Green, P.F., Duddy, I.R., Gleadow, A.J.W., and Tingate, P.R. (1985) Fission-track annealing in apatite: Track length measurements and the form of the Arrhenius plot. Nuclear Tracks, 10, 323–328.

Green, P.F., Duddy, I.R., Gleadow, A.J.W., Tingate, P.R., and Laslett, G.M. (1986) Thermal annealing of fission tracks in apatite. 1. A qualitative description. Chemical Geology (Isotope Geoscience Section), 59, 237–253.

Green, P.F., Duddy, I.R., Laslett, G.M., Hegarty, K.A., Gleadow, A.J.W., and Lovering, J.F. (1989) Thermal annealing of fission tracks in apatite. 4. Quantitative modelling techniques and extension to geological timescales. Chemical Geology (Isotope Geoscience Section), 79, 155–182.

Houpert, C., Hervieu, M., Groult, D., Studer, F., and Toulemonde, M. (1988) HREM investigation of GeV heavy ion latent tracks in ferrites. Nuclear Instruments and Methods in Physics Research, B32, 393–396.

Hughes, J.M., Cameron, M., and Crowley, K.D. (1989) Structural variations in natural F, OH, and Cl apatites. American Mineralogist, 74, 870–876.

Laslett, G.M., Green, P.F., Duddy, I.R., and Gleadow, A.J.W. (1987) Thermal annealing of fission tracks in apatite. 2. A quantitative description. Chemical Geology (Isotope Geoscience Section), 65, 1–13.

Laslett, G.M., Kendall, W.S., Gleadow, A.J.W., and Duddy, I.R. (1982) Bias in measurement of fission-track length distributions. Nuclear Tracks and Radiation Measurements, 6, 79–85.

Naeser, C.W., Crowley, K.D., McPherson, B.J., and Cameron, M. (1989) The relationship between fission-track length and fission-track density in apatite. Geological Society of America Abstracts with Programs, 21, 241–242.

Nye, J.F. (1957) Physical properties of crystals, 322 p. Oxford University Press, London.

Ravenhurst, C., Donelick, R.A., and Roden, M.K. (1989) Crystallographic orientation dependence of fission track annealing kinetics in apatite (abs.). EOS, 70, 1398.

Shannon, R.D. (1976) Revised effective ionic radii and systematic studies of interatomic distances in halides and chalcogenides. Acta Crystallographica, A32, 751–767.

Thiel, K., Bradley, J.P., and Spohr, R. (1988) On the nature of latent nuclear tracks in cosmic dust particles. Nuclear Tracks and Radiation Measurements, 15, 685–688.

Toulemonde, M., Balanzat, E., Bouffard, S., and Jousset, J.C. (1989) Structural modifications induced by electronic energy deposition during the slowing down of heavy ions in matter. Nuclear Instruments and Methods in Physics Research, B39, 1–6.

Turnbull, D. (1956) Phase changes. Solid State Physics, 3, 225–306.

Yada, K., Tanji, T., and Sunagawa, I. (1987) Radiation induced lattice defects in natural zircon ($ZrSiO_4$) observed at atomic resolution. Physics and Chemistry of Minerals, 14, 197–204.

Young, E.J., Myers, A.T., Munson, E.L., and Conklin, N.M. (1969) Mineralogy and geochemistry of fluorapatite from Cerro de Mercado, Durango, Mexico. U.S. Geological Survey Professional Paper 650-D, 84–93.

Manuscript received December 7, 1989
Manuscript accepted August 10, 1990

Appendix 1. Derivation of kinetic equation for axial shortening

Equations 1, 2, and 3 quantify the annealing kinetics of fission tracks in apatite, provided that the radial shrinkage of the disrupted zone (the quantity Δr^* in Eq. 1) can be expressed in terms of the defect elimination rate given by Equation 2 and the initial radial defect distribution given by Equation 3. To accomplish this, one first expresses the excess defect density N as a function of time t and fractional radial distance r as:

$$N(t,r) = N(0,r) + \int_0^t \left(\frac{dN}{d\tau}\right) d\tau$$

$$= N_0(1 - r)^{1/n} + \int_0^t \left(\frac{dN}{d\tau}\right) d\tau, \qquad \text{(A1)}$$

in which τ is a dummy variable of integration over time. The first term on the right side of Equation A1 is obtained by substitution from Equation 3. Then, recognizing that r^* at any time t is simply the value of r for which $N = N^*$, one can invert Equation A1 to express r^* as a function of t in this way:

$$r^*(t) = 1 - \left[\frac{N^* - \int_0^t \left(\frac{dN}{d\tau}\right) d\tau}{N_0}\right]^n. \qquad \text{(A2)}$$

The extent of radial shrinkage of the disrupted zone at any time t [that is, $\Delta r^*(t)$] is then the difference between the values of r^* obtained when Equation A2 is evaluated at $t = 0$ and at $t = t$:

$$\Delta r^*(t) = r^*(t) - r^*(0)$$

$$= \left[\frac{N^*}{N_0}\right]^n - \left[\frac{N^* - \int_0^t \left(\frac{dN}{d\tau}\right) d\tau}{N_0}\right]^n. \qquad \text{(A3)}$$

Substitution of the equation for the defect elimination rate (Eq. 2) into Equation A3 [making the dependence of temperature upon time explicit by replacing T with the notation $T(\tau)$], followed by substitution of Equation A3 into Equation 1, produces

$$l_{as} = l_0 + \frac{w}{\tan \phi}$$

$$\cdot \left\{\left[\frac{N^*}{N_0}\right]^n - \left[\frac{N^* - \int_0^t \left(\frac{-c\mathrm{k}}{\mathrm{h}}\right) T(\tau) \exp\left(\frac{-Q}{RT(\tau)}\right) d\tau}{N_0}\right]^n\right\}. \qquad \text{(A4)}$$

Equation A4 quantifies the rate of fission-track annealing in terms of time t; temperature T; the track width w and the taper angle ϕ, which together describe the geometry of the tip of the track; the quantities N_0, N^*, and n, which describe the initial radial defect distribution; and the quantities c and Q, which describe the defect-elimination rate and its temperature dependence. This equation can be reduced to one in which only three parameters appear, on the basis of a simplification that is justified both by the small-angle X-ray scattering and etching-rate studies of Dartyge et al. (1981), and by the linear relationship evident in the experimental data shown in Figure 3.

The simplification arises from the fact that the quantity (N^*/N_0), which is the ratio of the etching-threshold defect density to the initial density of defects at the axial center of the track, is a very small fraction. Dartyge et al. (1981, p. 5223) note that even values for the defect density that are quite small compared to the central value enhance the etching rate by a large factor; this is an indirect but observationally based indication that (N^*/N_0) is numerically very small. More direct evidence for the legitimacy of neglecting the (N^*/N_0) terms comes from the isothermal experimental data. If (N^*/N_0) is sufficiently small to be negligible by comparison to the other quantities in Equation A4, then Equation A4 reduces to

$$l_{as} = l_0 - \frac{w}{\tan \phi}\left[\int_0^t \left(\frac{c}{N_0}\right)\left(\frac{\mathrm{k}}{\mathrm{h}}\right) T(\tau) \exp\left(\frac{-Q}{RT(\tau)}\right) d\tau\right]^n. \qquad \text{(A5)}$$

For an isothermal anneal, Equation A5 has the form

$$l_{as} = l_0 - Ct^n, \qquad \text{(A6)}$$

in which C is a constant. This may be recast as:

$$\ln(l_0 - l_{as}) = \ln C + n \ln t \qquad \text{(A7)}$$

which accounts directly for the linear relationship inherent in the experimental results shown in Figure 3. The agreement between Equation A7 and the isothermal experimental data is empirical justification for neglecting the (N^*/N_0) terms in the course of the simplification used above to obtain Equation A5.

Defining the rate constant

$$A \equiv \frac{w}{\tan \phi} \cdot \left(\frac{c}{N_0}\right)^n \qquad \text{(A8)}$$

and extracting time-invariant factors from the integrand reduces Equation A5 to

$$l_{as} = l_0 - A\left(\frac{\mathrm{k}}{\mathrm{h}}\right)^n \left[\int_0^t T(\tau) \exp\left(\frac{-Q}{RT(\tau)}\right) d\tau\right]^n. \qquad \text{(A9)}$$